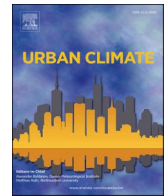




ELSEVIER

Contents lists available at [ScienceDirect](https://www.sciencedirect.com)

Urban Climate

journal homepage: www.elsevier.com/locate/uclim

Improving the accuracy of simplified urban canopy models for arid regions using site-specific prior information

Afshin Afshari^{a,*}, Nicolas Ramirez^b

^a Fraunhofer Institute for Building Physics, Germany

^b Engie Solutions Middle East, United Arab Emirates

ARTICLE INFO

Keywords:

Thermal network model
Urban Heat Island (UHI)
Urban canopy model
Town Energy Balance (TEB)

ABSTRACT

An overly complex urban climate/energy model would not be of much practical use in a decision support setting where a large number of year-long simulations are often necessary. While detailed modeling of urban momentum/energy exchanges can be attempted via Computational Fluid Dynamics (CFD) or mesoscale modeling, conducting multiple full year simulations in a design optimization or sensitivity analysis context is practically impossible. Furthermore, CFD models often do not consider climate/building energy exchanges. To address these limitations, stand-alone Urban Canopy Models (UCMs) have been developed, attempting to replace the full-fledged atmospheric representation with a computationally light equivalent. In this study, we investigate the impact of several modifications to a standalone Single-Layer Urban Canopy Model (SLUCM) for an arid region based on the prior availability of site-specific information. The suggested improvements are portable to SLUCM schemes incorporated within mesoscale models. The SLUCM will undergo several improvements and each variant will be evaluated based on its ability to predict UHI intensity and air-conditioning energy demand. Three original SLUCM improvements are covered in the present study. (1) We use actual radiation parameters instead of those generated for idealized geometries. It is shown that, in the absence of this improvement, standard UCMs can underestimate the average urban heat island intensity by 5% if using the Town Energy Balance (TEB) radiation scheme or overestimate it by 7% if using the Square Prism Urban Canopy (SPUC) radiation scheme. (2) We use the results of a prior steady-state RANS (Reynolds-Averaged Numerical Simulation) simulation to replace some of the default morphological parameters of the UCM by the more accurate values derived from the RANS results. It is shown that, in the absence of this improvement, standard UCMs using default empirical relations can overestimate the average urban heat island intensity by up to 22%. (3) Instead of using the empirically calculated default value of the urban canyon wind speed, we estimate it directly from the concomitant rural value using a regression model trained by historical measurements. It is shown that, in the absence of this improvement, standard UCMs can underestimate the average canyon wind velocity by more than 12%, although the other indicators (UHI, cooling demand) are not significantly affected.

* Corresponding author.

E-mail address: afshin.afshari@ibp.fraunhofer.de (A. Afshari).

<https://doi.org/10.1016/j.uclim.2020.100722>

Received 29 June 2020; Received in revised form 8 September 2020; Accepted 15 October 2020

Available online 6 November 2020

2212-0955/© 2020 The Authors.

Published by Elsevier B.V. This is an open access article under the CC BY license

(<http://creativecommons.org/licenses/by/4.0/>).

Nomenclature

Symbol	Designation	Unit
Constants		
σ	Stefan-Boltzmann constant: $5.67 \cdot 10^{-8}$	W/m^2K^4
λ	Latent heat of vaporization: $2.436 \cdot 10^6$	J/kg
ρ	Density: 1000 for water; 1.2 for air	kg/m^3
c_p	Specific heat at constant pressure: 4180 for water; 1000 for air	J/kgK
κ	Von Karman constant: 0.40	—
R	Ratio of the drag coefficients for momentum and heat in the neutral limit: 0.74 adjusted to 0.95	—
Variables		
z	Height from the ground	m
T	Temperature	$^{\circ}C$ or K
θ	Potential temperature	$^{\circ}C$ or K
q	Humidity mixing ratio	g/kg
p	Gas pressure	kPa
I_h	Horizontal solar irradiance	W/m^2
I_v	Vertical solar irradiance	W/m^2
u	Horizontal wind velocity	m/s
w	Vertical wind velocity	m/s
\dot{Q}_a	Anthropogenic heat rate per unit of site surface area	W/m^2
Q_c	Annual cooling load per unit of site gross floor area	kWh/m ²
H	Vertical turbulent sensible heat flux	W/m^2
E	Vertical turbulent water vapor flux	kg/m^2s
Parameters		
h (no subscript)	Plan area weighted average height of urban canopy roughness elements	m
λ_p	Plan area index of the urban area	—
λ_F	Frontal area index of the urban area	—
l	Length of the average cuboid roughness element	m
w	Width of the average street	m
A	Area	m^2
z_0	Roughness height for the urban canopy	m
d	Zero-plane displacement height of the urban canopy	m
τ	Urban canopy shear stress	Pa
u_*	Urban canopy friction velocity	m/s
θ_*	Turbulent vertical flux of temperature normalized by u_*	K
q_*	Turbulent vertical flux of humidity normalized by u_*	g/kg
h (with subscript)	Heat conductance coefficient (conductive/convective/radiative)	W/m^2K
C	Thermal capacitance	J/K
f	Infiltration rate	Air Changes per Hour
e	Chiller efficiency (Coefficient of Performance)	—
ϵ	Emissivity	—
α	Albedo (solar reflectance)	—
L	Monin-Obukhov length	m
Ri	Richardson number	—
C_D	Drag coefficient	—
C_H	Bulk sensible heat transfer coefficient (Stanton number)	—
C_Q	Bulk latent heat transfer coefficient (Dalton number)	—
Ψ	Monin-Obukhov stability function (momentum, sensible, latent)	—
Subscripts		
w	Wall	
r	Roof	
g	Glazed surfaces	
p	Paved surfaces	
v	Vegetation	
e	Earth (below paved surfaces)	
s	Sky	
i	Indoor	
o	Outdoor	
f	Floor	
t	Total site	
a	Ambient or rural	
u or can	Urban canyon	
c	Cooling	
ref	Reference height, i.e., top of the inertial sublayer (typically, $3h$)	
top	Top of the urban canopy i.e., roof-level	
b	Blending height (typically, $h + 1.5w$)	

1. Introduction

Urbanization results in larger cities' and denser urban tissue. The temperature of the air in densely built areas is generally higher than in the surrounding rural hinterland, a phenomenon known as the "Urban Heat Island" or UHI (Landsberg, 1981). The UHI creates demand for more indoor cooling in hot climate and increases the mortality rate during heat waves (Gabriel and Endlicher, 2011). The

temperature differential can reach a maximum 12 °C (Oke, 1973). Many researchers have worked on modeling UHI and the most accurate way of doing so is via CFD. However, the construction, simulation and validation of such models present significant challenges (Mirzaei, 2015). An overly complex urban climate/energy model would not be of much practical use in a design optimization or sensitivity analysis setting where multiple simulations for a full year are often necessary. While detailed modeling of urban momentum/energy exchanges can be attempted via CFD, simulating a transient CFD model of a realistic urban domain for a full year is practically impossible. Furthermore, a comprehensive CFD model implementing the dynamic coupling of urban microclimate to building heat transfer is, currently, still a research topic (e.g., PALM/PALM-4 U; Maronga et al., 2020).

To address these limitations, simplified UCMs have been developed. In these simplified schemes buildings are not explicitly represented. The urban fabric is characterized only in average. When used in combination with a mesoscale model, one of the goals of the simplified UCM is to provide an accurate estimation of the urban canopy thermal conditions and to study the sensitivity of said conditions to urban morphology and surface properties (Tsiringakis et al., 2019). UCMs are contingent on the assumption of an idealized form for the urban roughness elements: infinite rows of buildings, regular array of cuboid building, etc. Within the urban canopy, the complexity and computational speed of these models is significantly reduced thanks to the implementation of a simplified representation of momentum transfers. Concurrently, the spatial organization of the surfaces (slopes, orientations, shape factors), and their physical characteristics (albedo, emissivity, thermal conductivity) are simplified as well. In particular, the models often rely on very rough estimations of short-wave (solar) and long-wave (infrared) radiation heat transfer.

Two main categories of UCM are described in the literature, single layered and multilayer. The SLUCM schemes can be as simple as modifications to the surface characteristics of the urban landscape (Liu et al., 2006; Grossman-Clarke et al., 2005) or more sophisticated urban models with explicit modeling of the urban roughness such as the TEB by Masson (2000) or the SPUC by Aoyagi and Seino (2011). These single-layer UCMs focus on the overall exchange of heat, momentum, and moisture with the first level of the atmosphere right above the urban canopy. Boundary conditions are defined at a reference height above the urban canyon, typically about two to three times the average building height. Exchange of momentum is parametrized using the Monin-Obukhov Similarity Theory (MOST) first described by Monin and Obukhov (1954), while canopy wind speed is derived from simple empirical relations. Air temperature and humidity are assumed to be uniform in the canyon. The TEB scheme is the most often used SLUCM. It only models one generic roof, one generic wall and one generic road. Averaging is performed over all directions in order to keep only these generic surfaces. Kusaka et al. (2001) proposed an urban canopy model similar to TEB, but it incorporated solar calculations for specific orientations of the urban canyon. The Multi-Layer UCM (MLUCM) schemes are typically parameterized in terms of the horizontally averaged flow and scalar transport (Martilli et al., 2002). The boundary conditions of the MLUCM are provided at different vertical levels inside the urban canyon, generally by a mesoscale model. This approach allows a higher resolution of atmospheric processes, but it requires a fine discretization of the mesoscale model near the surface, which significantly increases the computational cost of simulations. MLUCMs require the resolution of prognostic equations for both momentum and turbulent kinetic energy (TKE). Santiago and Martilli (2010) and Simón-Moral et al. (2014) used RANS CFD simulations of idealized urban configurations determine drag coefficients and turbulent length scales as a function of height. Nazarian et al. (2020) have recently suggested parametrizing the UCM using Large Eddy Simulation (LES) instead of RANS given the latter's inaccuracy when it comes to representing turbulent flows. MLUCMs, at the expense of a significantly higher computational cost, theoretically offer a better treatment of canopy physics. Nonetheless, there is currently no clear consensus on the superiority of MLUCMs over SLUCMs among researchers modeling UHI in different cities (e.g.: Jänicke et al., 2017); although presumably if the canyon wind speed accuracy is a primary concern, MLUCM should be preferred. Mesoscale models, such as WRF, the Weather Research and Forecasting (Chen et al., 2011; Powers et al., 2017) can be fitted with a UCM to represent sub-grid scale urban processes. However, due to the computational intensity of the atmospheric scheme, annual assessments and iterative optimization of design features or sensitivity analysis of building/surface properties are currently out of reach for anyone who lacks access to high performance computing.

Currently, the most convenient option for the research-minded urban planning practitioner is to use stand-alone UCMs. Indeed, urban planners often require multiple year-long simulations in order to evaluate and optimize competing design (new urban area) or retrofit (existing urban area) alternatives. These further reduce the computational time by inferring the top of the canopy boundary conditions from a single measurement point located outside the urban canopy. In this way, the costly detailed atmospheric modeling is circumvented. Most often these standalone UCMs rely on standard rural weather measurements (at 2 and 10 m) and derive top of the canopy conditions using simplified schemes (e.g.: Bueno et al., 2013; Le Bras and Masson, 2015; Afshari, 2017). Huang et al. (2020), on the other hand, directly use a rooftop weather station.

In this study, we choose to focus on improving a TEB-style SLUCM simulated in standalone mode. The more sophisticated MLUCMs present a more intricate coupling with the atmosphere and are, therefore, not good candidates for standalone simulation. To facilitate this study, the comprehensive sensible/latent fully validated SLUCM of Afshari (2017) has been selected as baseline model. It will undergo several improvements and each variant will be evaluated on the basis of its ability to predict UHI intensity and buildings' air-conditioning energy demand. The suggested improvements are of course portable to SLUCM schemes incorporated within mesoscale models, although their impact in such a setting has not been investigated in the present study. Since the study refer to an arid region, the soil moisture is not considered.

The novel SLUCM improvements covered in the present study include:

- Using actual radiation parameters instead of those generated for idealized geometries
- Using the results of a prior steady-state RANS simulation for the urban domain of interest to modify the default values of some morphological parameters required by the SLUCM (existing urban area only)

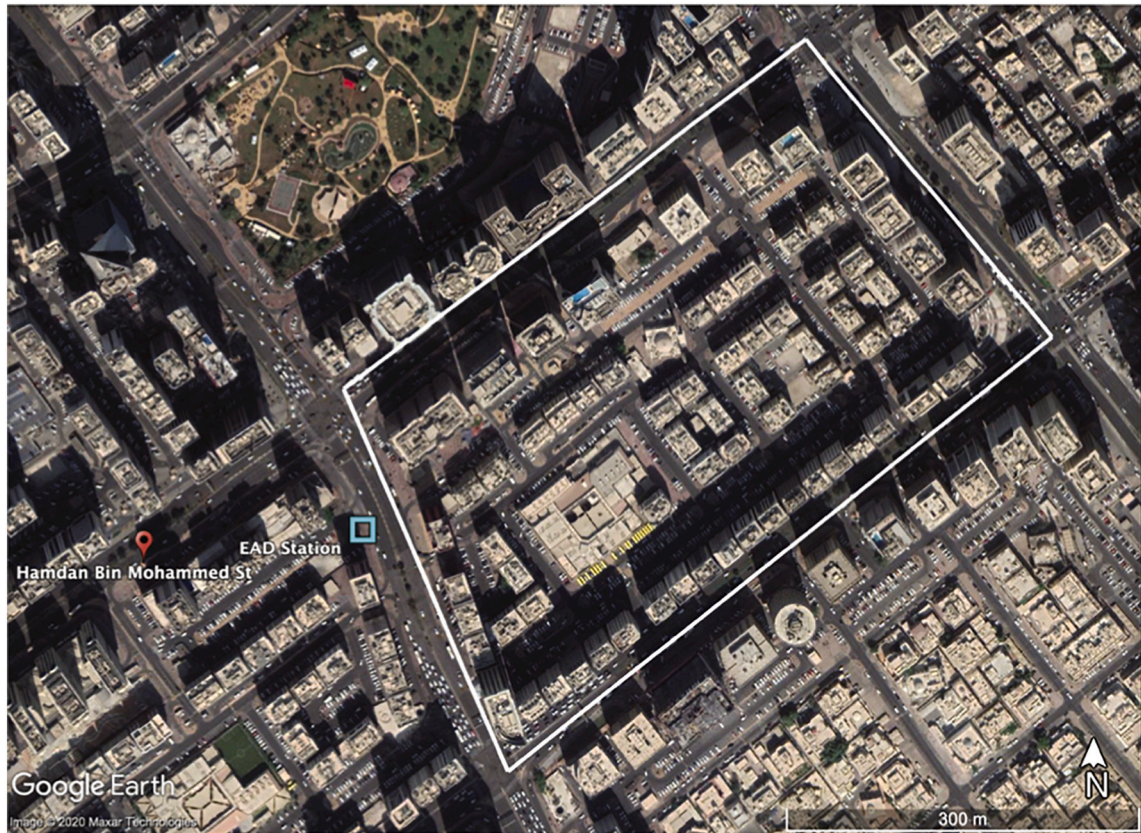


Fig. 1. Selected site for the assessment of the improvements. The position of the urban monitoring station is marked by a blue square. (For interpretation of the references to colour in this figure legend, the reader is referred to the web version of this article.)

- Inferring the urban canyon wind speed directly from the rural station value instead of using the default empirically calculated value (existing urban area only)

In [Section 2](#), we describe the urban site selected to investigate the impact of these improvements. In particular, the site's morphology (actual and idealized), the thermophysical properties of the urban structures and the sources of weather data are described. In [Section 3](#), a brief description of the modeling methodology is provided. In [Section 4](#), the suggested improvements are described in detail. In [Section 5](#), the impact of each improvement is shown and discussed. In the last section, we present the main conclusions of the study and suggest tracks for future research.

2. Urban site

2.1. Location

We evaluate the impact of the proposed improvements using, as case study, a district in Abu Dhabi, UAE referred to as district E3 (enclosed by a white box [Fig. 1](#)). The district is composed of 67 mixed-use buildings. A comprehensive energy audit of the whole district was conducted in 2011. The location of urban weather monitoring station of the Environmental Agency which will be used later is shown as a blue box on [Fig. 1](#).

2.2. Geometric and thermophysical characterization

The simplest morphological representation of the urban canopy relies on 3 primary parameters: average building height h , plan area index λ_p and frontal area index λ_f . h is the area-weighted average height of all buildings in the studied region. λ_p is the ratio of the plan area of buildings over the total area of the site. Finally, λ_f is the ratio of average vertical area of roughness elements (buildings) opposing the urban wind flow over the total site area. The latter parameter is, in the general case, dependent on the actual wind flow

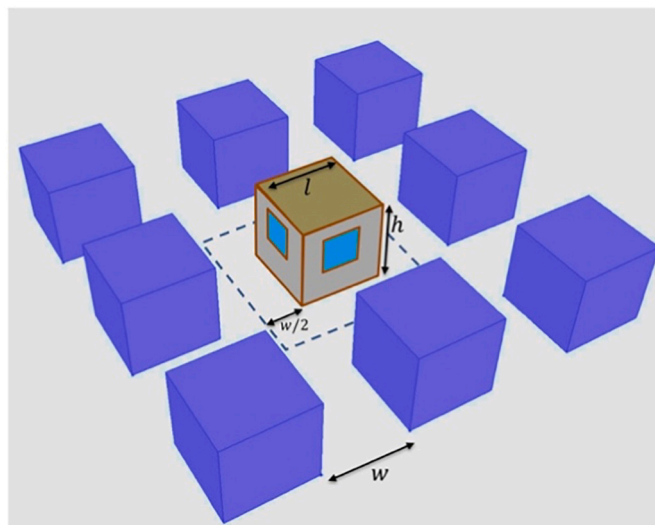


Fig. 2. Schematic representation of the simplified geometry.

direction. However, in most studies it is approximated as 1/4th of the vertical façade area divided by the site area. Instead of attempting to model the full geometric complexity of the actual site, we examine, as is customary in UCMs, an equivalent regularized arrangement of buildings and streets that is based on the morphological parameters h , λ_p and λ_f of the actual domain. Specifically, we assume a regular array of identical buildings with a square footprint $l \times l$ interlaced by streets having the same width w (see Fig. 2). Then, from the primary parameters, secondary parameters l and w can be derived. These secondary parameters are necessary for the calculation of the default sky view factors. Thereafter, using the symmetry properties of the simplified regular geometric representation, the urban domain model is reduced to a single regularized building surrounded by half the width of the regularized street. From this, we can derive A_t the total area of the domain to be modeled.

The values of these parameters for district E3 of Abu Dhabi, as computed from GIS data, are listed in Table 1.

Typical building thermo-physical parameters are based on a previous study by Afshari et al. (2014) as well as on the results of an energy audit of the district E3 (Abu Dhabi Municipality, 2011). The properties of the prototypical building and paved street in the downtown district are displayed in Table 2. The anthropogenic heat profile used here is the one derived by Afshari et al. (2018). It is not discussed here in any detail. Further details about the thermophysical parameters are provided in Afshari (2017).

2.3. Weather data

Although a wealth of high accuracy urban and rural data in and around Abu Dhabi is available, for the sake of reproducibility, in our year-long simulations, we use the standard hourly weather file for Abu Dhabi produced by the International Weather for Energy Calculations (IWECC). The IWECC data is readily available on the web and is often used in building energy models.

For the derivation of the regression model relating rural weather to urban canyon wind speed, we use actual measured rural/urban data. We could not use the IWECC data for this purpose since it only contains rural measurements. The actual rural data used for this regression is from the year 2010 and was measured at a location near the international airport. The rural weather station is isolated and at a distance from Abu Dhabi downtown. The actual urban data is from the same year and was measured by the Environmental Agency's roadside monitoring station located along a main corridor close to the E3 district (blue square in Fig. 1). The predominant wind direction at the rural location is north-north-west, with an average wind speed of 2.83 m/s at a height of 10 m above ground. The predominant wind direction at the urban station is more or less aligned with the main corridor—only slightly deviating from the north—with an average wind speed of 1.70 m/s.

3. Modeling principle

As mentioned previously, in this study, we use the standalone SLUCM of Afshari (2017). Although this SLUCM is capable of modeling building-integrated greenery, that feature will not be activated here. On the other hand, latent energy exchanges within and outside the building are fully accounted for by the model and humidity mixing ratio is one of the canopy-top boundary conditions (together with temperature and wind speed). The model will undergo several improvements and each variant will be simulated over a typical year and subsequently evaluated on the basis of its ability to predict average diurnal UHI intensity and air-conditioning energy

Table 1
Main morphological parameters for the island of Abu Dhabi (determined from GIS data).

h	36.7 m
λ_p	0.239
λ_f	0.282
$l = h\lambda_p/\lambda_f$	31.1 m
$w = l(1/\sqrt{\lambda_p} - 1)$	32.5 m
$A_t = (l + w)^2$	4045 m ²

demand. Given the location of the urban site, indoor space heating energy is negligible. Similarly, rain is rare enough in the region that its effect need not be modeled.

3.1. Approach

We use a dynamic thermal network lumped-parameter model to represent the thermal exchanges between buildings and the urban environment. This lumped-parameter model is based on an electrical analogy whereby a resistance represents the inverse of thermal conductance between two nodes and a capacitance represents the thermal mass of a node. Temperature is analogous to electric potential difference while heat flux is analogous to electric current (e.g., Pinterić, 2017). As shown on Fig. 3, the thermal interactions are mainly mediated by the urban canyon air, itself in contact with the paved surfaces as well as the free atmosphere above the canopy.

In addition to sensible heat network shown in Fig. 3, the UCM computes, in a coupled manner, a latent heat network model for latent heat (not shown here). That latent component of the UCM is dynamically coupled with the sensible component's evapotranspiration flux and infiltration latent heat flux on one hand and the ambient humidity level (prescribed by the weather file) on the other. This UCM has many parameters, in particular sophisticated aerodynamic and evapotranspiration schemes are implemented. A soil moisture model is also implemented but not used in this case study since, due to the arid climate, the soil is almost always dry, down to

Table 2
Specifications for the building and the road.

Urban Domain Properties	Value
Floor to ceiling height (m)	2.85
Floor/roof thickness (m)	0.35
Paved street thickness (m)	1.00
Roof U-value (W/m ² K)	1.29
Wall U-value (W/m ² K)	2.25
Window U-value including films (W/m ² K)	3.88
Paved street U-value (W/m ² K)	1.20
Glazing Ratio	33%
Solar Heat Gain Coefficient (SHGC)	0.75
Roof solar reflectance (albedo)	0.26
Wall solar reflectance (albedo)	0.30
Glazing solar reflectance (albedo)	0.15
Paved street solar reflectance (albedo)	0.10
Roof emissivity	0.90
Wall emissivity	0.90
Glazing emissivity	0.84
Paved street emissivity	0.95
Roof mass heat capacity (kJ/m ³ K)	1.2 * 10 ³
Wall mass heat capacity (kJ/m ³ K)	1.2 * 10 ³
Paved street mass heat capacity (kJ/m ³ K)	1.6 * 10 ³
Indoor CHTC ^a (W/m ² K)	5
Roof-air CHTC (W/m ² K)	5.6 + 4 V (Jürges, 1924)
Wall-air CHTC (W/m ² K)	5.6 + 4 V (Jürges, 1924)
Street-air CHTC (W/m ² K)	5.6 + 4 V (Jürges, 1924)
People heat gains (W/m ²)	Max value 5 (daily schedule per Afshari, 2017)
Equipment/lighting heat gains (W/m ²)	Max value 5 (daily schedule per Afshari, 2017)
Latent portion of internal heat gains (W/m ²)	20%
Vehicular anthropogenic heat gains (W/m ²)	Max value 21.6 (daily schedule per Afshari, 2017)
Latent portion of anthropogenic gains (W/m ²)	9%
COP ^b	2.5
Infiltration (Air Changes per Hour)	0.5
Fraction of chiller waste heat rejected into urban canyon	100%

^a CHTC: Convective Heat Transfer Coefficient.

^b COP: Coefficient of Performance of the chiller.

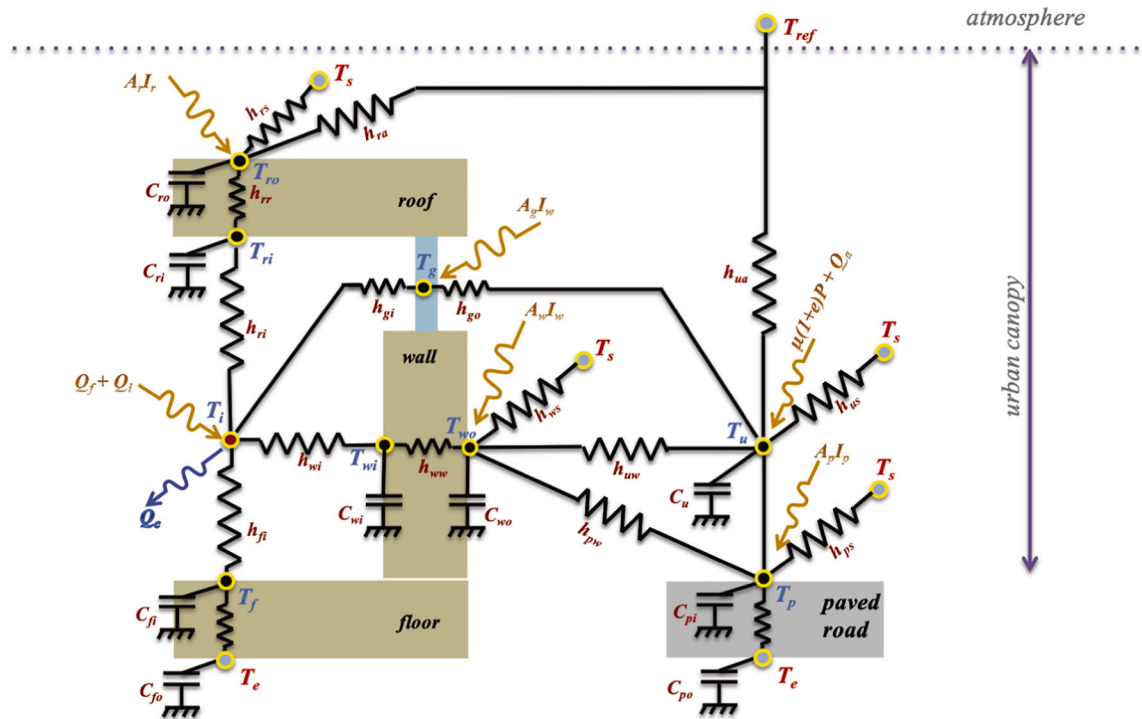


Fig. 3. The urban canopy model. Parameters h_{ij} and C_{ij} are, respectively, thermal conductance between two nodes and thermal mass of a node (the thermal reference point is 0 K). For the description of the subscripts, refer to the nomenclature.

a depth of several meters. Similarly, vegetation is scarce in the downtown area of Abu Dhabi and is assumed to have negligible effect on the UHI.

The sensible-latent thermal network model is fully specified using a combination of coding and graphical representation. The energy exchanges are resolved in MATLAB®/SIMSCAPE™ using ode15s, the iterative variable-time-step solver of stiff ordinary differential equations. The simulation runs for every hour of a standard year (8760 h) and is driven by standard IWEC hourly weather data for Abu Dhabi airport. The main outcomes are cooling electricity and Urban Heat Island (UHI) intensity. The latter defines the urban-rural air temperature differential.

The modeling approach is based on deriving wind speed, virtual temperature and humidity mixing ratio at the reference height above the rural ground. While for calculating the reference wind speed, we use a neutral stratification assumption, when it comes to estimating the reference virtual temperature, a more sophisticated approach is adopted as will be discussed below. As for the humidity mixing ratio at the reference height, in agreement with studies such Melecio-Vázquez et al. (2018) we assume that it is approximately equal to the value measured at the rural weather station. Once these values are determined, we assume that they also prevail, unchanged, above the urban canopy, at height z_{ref} (although u_{ref} is slightly adjusted to take account of the differential roughness; see below). From here we determine, using the Mascart approximation, the coefficients C_D (drag coefficient), C_H (Stanton number or bulk sensible heat transfer coefficient) and C_Q (Dalton number or bulk latent heat transfer coefficient) at the reference height (for simplicity, C_Q is set equal to C_H). The heat exchange between the lowest level of the atmosphere ($z = z_{ref}$) and the urban canyon air, assumed to be thermally homogeneous, is then determined according.

The building model is sophisticated enough for the purpose of characterizing average UHI and city-wide air-condition load. For details on some other aspects of the model such as the evapotranspiration scheme, the sky temperature, the soil temperature, etc., the reader is referred to Afshari (2017). For the anthropogenic heat profile due to motorized traffic, please refer to Afshari et al., 2018. Thanks to the nature of network modeling, it is not necessary to determine all unknowns sequentially. Instead once the formulae relating the variables to each other are set (and they can be linear or nonlinear), the resolution of all unknowns at a given time step proceeds iteratively. This increases the computational intensity, but software development, debugging and maintenance become much easier.

3.2. Morphological parameters

Morphological parameters are aerodynamic properties of a site determined through the analysis of its surface form. The most important morphological parameters are:

- The roughness length for momentum z_0 (its value is about one tenth of the average roughness element height).

- The zero-displacement height for momentum d (its value is about three fourth of the average roughness element height).
- The blending height or depth of the roughness sublayer z_b .
- The reference height z_{ref} : The height of the first level of the atmosphere, i.e., top of the inertial sublayer.
- The neutral drag coefficient C_{DN} : Drag coefficient in neutral stratification; usually evaluated at the reference height.
- The neutral Stanton number C_{HN} : Stanton number in neutral stratification; usually evaluated at the reference height.

Empirical determination of the morphological parameters is more convenient than the alternative approach of using field observations or CFD simulations of wind or turbulence in order to derive these properties from the theoretical logarithmic wind profile law. The empirical formulae, however, are often based on experimental wind tunnel data pertaining to idealized flows over regularly spaced arrays of identical roughness elements. [Grimmond and Oke \(1999\)](#) present a comprehensive list of empirical morphometric determination formulae and conduct a sensitivity analysis of the different methods. In the standard model, we use the following formulations:

- The default values of z_0 and d are prescribed in agreement with [Masson \(2000\)](#):

$$d = \frac{2}{3}h$$

$$z_0 = \frac{h}{10}$$

- The default value of z_b is prescribed according to [Raupach et al. \(1980\)](#):

$$z_b = h + 1.5w$$

- The default value of z_{ref} is prescribed according to [Panagiotou et al. \(2013\)](#):

$$z_{ref} = 3h$$

- The coefficient a of the exponential profile of the wind velocity in the urban canyon (e.g., [Cionco, 1965](#)). The default value is prescribed according to [Masson, 2000](#):

$$a = \frac{h}{4w}$$

- The ratio of $u_{ref} = u(z_{ref})$ over rural wind speed u_a . Since we need u_{ref} over the urban canopy, we use the adjustment suggested by [Erell et al. \(2010\)](#) for adjacent surfaces with different roughness based on the presumed unicity of the geostrophic wind velocity above neighboring rural and urban regions:

$$\frac{u_{*2}}{u_{*1}} = \left(\frac{z_{02}}{z_{01}} \right)^{0.09}$$

Therefore, the default value of u_{ref} , assuming neutral stratification, is:

$$\frac{u_{ref}}{u_a} = \left(\frac{z_0}{z_{0r}} \right)^{0.09} \frac{\ln[(z_{ref} - d)/z_0]}{\ln[(z_m - d_r)/z_{0a}]}$$

- z_m is the height of the rural wind velocity sensor ($z_m = 10 \text{ m}$). z_{0a} is the roughness height of the rural site ($z_{0a} = 0.08 \text{ m}$) according to [Ramirez et al. \(2018\)](#). The rural displacement height is derived from z_{0a} : $d_r = (3/4)(10 \cdot z_{0a}) = 0.533 \text{ m}$.
- The ratio of the friction velocity u_* over u_{ref} . u_{ref} is assumed to be the same over rural and urban areas. The original UCM value is given by [Mascart et al. \(1995\)](#):

$$\frac{u_*}{u_{ref}} = \sqrt{C_{DN}(z_{ref})}$$

where $C_{DN}(z_{ref})$, the neutral conditions drag coefficient, is:

$$C_{DN}(z_{ref}) = \frac{\kappa}{\ln[z_{ref}/(d - z_0)]}$$

κ , the von Karman constant, is taken equal to 0.40 throughout this study.

- The ratio of the roof-level velocity u_{top} over u_{ref} . The default value is, in accordance with Masson (2000):

$$\frac{u_{top}}{u_{ref}} = \frac{2}{\pi} \frac{\ln \left[\frac{h/3}{z_0} \right]}{\ln \left[\frac{(z_{ref}-d)+h/3}{z_0} \right]}$$

- The ratio of the urban canopy average horizontal velocity u_{can} over u_{ref} . The default value is, in accordance with Masson (2000):

$$\frac{u_{can}}{u_{ref}} = \frac{2}{\pi} e^{-\frac{h}{40}} \frac{\ln \left[\frac{h/3}{z_0} \right]}{\ln \left[\frac{(z_{ref}-d)+h/3}{z_0} \right]}$$

Note: the total canyon wind velocity is $\sqrt{u_{can}^2 + u_s^2}$

- C_{dh} : drag coefficient at height h (average height of buildings). The default value is 1.20, in agreement with Bottema (1997).

3.3. Top of the canopy boundary conditions

In order to calculate the heat transfer between the urban canopy and the atmosphere, the model needs an estimate of the bulk heat transfer coefficient C_H . According to the standard Monin-Obukhov Similarity Theory, within the surface layer, but above the roughness sublayer, the following equations can be used to determine average wind speed u , potential temperature θ and humidity mixing ratio q (e.g., Louis, 1979):

$$u(z) = \frac{u_*}{\kappa} \left[\ln \left(\frac{z-d}{z_0} \right) - \Psi_M \left(\frac{z-d}{L} \right) \right]$$

$$\Delta\theta(z) = \frac{\theta_*}{\kappa/R} \left[\ln \left(\frac{z-d}{z_{0H}} \right) - \Psi_H \left(\frac{z-d}{L} \right) \right]$$

$$\Delta q(z) = \frac{q_*}{\kappa/R} \left[\ln \left(\frac{z-d}{z_{0Q}} \right) - \Psi_Q \left(\frac{z-d}{L} \right) \right]$$

Ψ_M , Ψ_H and Ψ_Q are stability functions for momentum, sensible heat and latent heat. L , the Obukhov length, accounts for the effects of stability: $L = \bar{\theta} u_*^2 / \kappa g \theta_*$. $\Delta\theta = \theta - \theta_0$ where θ_0 is the potential temperature at height $d + z_{0H}$ assumed to be the same as the ground temperature. $\Delta q = q - q_0$ where q_0 is the saturated specific humidity for the ground temperature. u_* is the friction velocity: $u_* = \sqrt{\tau/\rho}$. τ is the urban surface shear stress: $\tau = \rho u_*^2$. The temperature scale θ_* is the turbulent vertical flux of temperature $-\overline{w'\theta'}$ normalized by u_* : $\theta_* = -\overline{w'\theta'}/u_*$. The humidity scale q_* is the turbulent vertical flux of humidity $-\overline{w'q'}$ normalized by u_* : $q_* = -\overline{w'q'}/u_*$. R , ratio of the drag coefficients for momentum and heat in the neutral limit, was estimated by Businger et al. (1971) to be 0.74. However, he assumed $\kappa = 0.35$. For $\kappa = 0.40$, the modified value of R is 0.95 (Hogstrom, 1988).

The surface momentum, sensible heat and latent energy fluxes τ , H and λE can be expressed as (Beljaars and Holtslag, 1991; Jacobson, 2005):

$$\tau = -\rho_{air} \overline{u'w'} = \rho_{air} u_*^2 = -\rho_{air} C_D u_*^2$$

$$H = \rho_{air} c_p \overline{w'\theta'} = -\rho_{air} c_p u_* \theta_* = -\rho_{air} c_p u C_H \Delta\theta$$

$$\lambda E = \lambda \rho_{air} \overline{w'q'} = -\lambda \rho_{air} u_* q_* = -\lambda \rho_{air} u C_Q \Delta q$$

where ρ_{air} is the density of air in kg/m^3 , c_p is the specific heat of air in J/kgK and λ is the latent heat of water in J/K . In other words, knowing the coefficients C_D , C_H and C_Q we can calculate the aerodynamic resistances for momentum, sensible heat and latent heat fluxes. We assume hereafter that $C_Q \approx C_H$.

The stability functions are usually obtained empirically by fitting field experiment data for certain specific configurations. A more convenient formulation consists in expressing the coefficients C_D and C_H using the previous formulas (Garratt, 1992):

$$C_D = \frac{\kappa^2}{\left(\ln \left(\frac{z-d}{z_0} \right) - \Psi_M \right)^2} = \left(\frac{u_*}{u} \right)^2$$

$$C_H = \frac{\kappa^2 / R}{\left(\ln \left(\frac{z-d}{z_0} \right) - \Psi_M \right) \left(\ln \left(\frac{z-d}{z_{0H}} \right) - \Psi_H \right)}$$

The flux coefficients C_D and C_H do not depend on wind speed and are only weakly dependent on height, roughness, and typical atmospheric stability conditions. Mascart et al. (1995) developed empirical expressions for C_D and C_H . These empirical formulas express each coefficient as a function of its value in ‘neutral conditions’ (no buoyancy):

$$C_D = C_{DN} F_M$$

$$C_H = C_{HN} F_H$$

Further details are provided in the Annex.

In this study, in order to calculate the heat exchange between the urban canopy and the atmosphere, we use Mascart’s approximation of C_D and C_H . For the calculation of the heat exchange between urban surfaces and the canopy air, we use the Jürges (1924) convective heat transfer coefficients.

In order to derive the temperature at the first level of the atmosphere, we differentiate between day-time and night-time. In day-time, we use radiosonde data measured at the Abu Dhabi airport (location OMAA) very near to our rural weather station. The mid-day potential temperature as a function of height was retrieved (UWYO, 2020) and averaged over the full year 2019. The resulting vertical profile is presented in Fig. 4. The average mid-day gradient near the surface (between the lowest measurement level and a height of 65 m) is approximately -22.4 K/km .

The gradient at sunrise gradually changes from its value at the end of the previous night to this value at mid-day. Thereafter, it gradually changes to its prescribed value at the start of the night period. The night-time vertical variation of the potential temperature is determined following Stull (2017) by assuming a stable atmospheric boundary layer. Under these conditions the potential temperature profile is almost exponential with height:

$$\Delta\theta(z) = \Delta\theta_s \cdot e^{-z/H_e}$$

$\Delta\theta(z)$ is the potential temperature difference between the air at height z and the air in the residual layer: $\Delta\theta(z) = \theta(z) - \theta_{RL}$. Its value near the ground, $\Delta\theta_s$ is:

$$\Delta\theta_s = Q_{Ak}/H_e$$

Q_{Ak} is the accumulated cooling per unit surface: $Q_{Ak} = F_H \cdot t_{\text{night}}$. F_H is the night-time heat flux from the air to the surface, divided by the product of air density and specific heat ($\rho_{\text{air}} C_p$). F_H is negative and approximately constant. Stull (2017) suggests a typical value of $-0.041 \text{ K} \cdot \text{m} \cdot \text{s}^{-1}$. In our case, measurements of surface-to-sky long wavelength radiation at the rural site reveal F_H to be closer to $-0.025 \text{ K} \cdot \text{m} \cdot \text{s}^{-1}$. H_e is an e-folding height for the exponential curve. It can be approximated as:

$$H_e \approx a \cdot u_{RL}^{3/4} \cdot t_{\text{night}}^{1/2}$$

where $a = 0.15 \text{ m}^{1/4} \text{ s}^{1/4}$ for flow over a flat prairie, u_{RL} is the wind speed in the residual layer and t_{night} is the time in seconds since sunset. Assuming that the temperature at the surface is the same as the one measured by the rural weather station, we can derive $\theta_{RL} = \theta(z_m) - Q_{Ak}/H_e$. Finally:

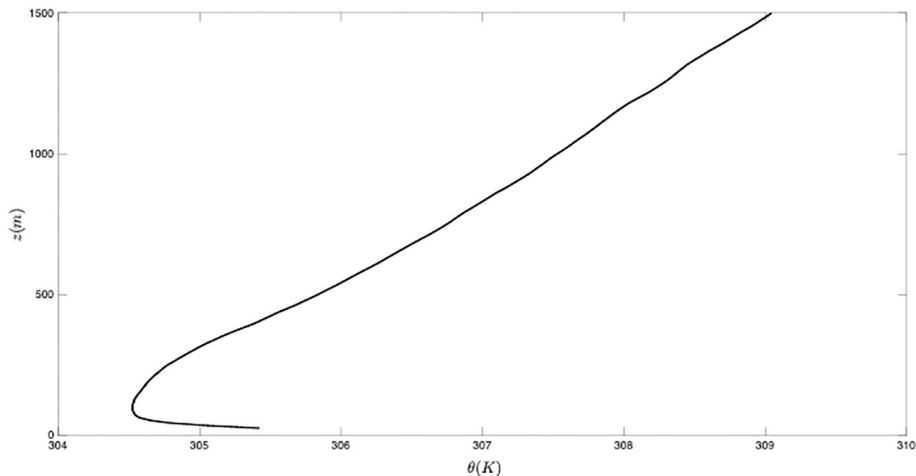


Fig. 4. Average vertical profile of potential temperature $\theta(z)$ at mid-day for Abu Dhabi airport up to a height of 1500 m (2019 data).

$$\theta(z_{ref}) = \frac{Q_{Ak}}{H_e} e^{-z_{ref}/H_e} + \theta_{RL} = \theta(z_m) + \frac{Q_{Ak}}{H_e} (e^{-z_{ref}/H_e} - 1)$$

4. Suggested improvements

Three improvements are described in this section:

- Using actual radiation parameters instead of those generated for idealized geometries
- Using the results of a prior steady-state flow-only RANS simulation for the urban domain of interest to modify the default values of some morphological parameters
- Inferring the urban canyon wind speed directly from the rural station value

The first improvement is applicable to both new and existing urban areas while the last two improvements are only applicable to sensitivity study or retrofit analysis (cool/green surfaces, rooftop photovoltaics, building envelope/HVAC upgrade, etc.) within an existing urban area. The additional effort required for the implementation of these improvements is often justified since, for both applications, the simulation of tens or hundreds of scenarios, each conducted over a full-year, may be required. The suggested improvements are independent of each other and it is possible, depending on the specific circumstances/limitations of a given case study, to choose only one or two out of three.

4.1. Radiation

In this study, we assess the comparative validity of the radiation heat transfer parameters (net incident global irradiance on urban surfaces, and surface view factors) approximated by several simplified modeling approaches in comparison to exact solutions that we calculate for an actual urban district.

Radiation heat transfer is comprised of shortwave and longwave components. Shortwave radiation can be direct or diffuse, while longwave radiation is diffuse. Most of the energy of solar radiation is within the short wavelength range (hereafter referred to as “shortwave radiation”). Once in the Earth’s atmosphere, clouds and the surface absorb some of the energy of solar radiation. The remainder contributes to heating the ground and other urban surfaces. In turn, these surfaces re-emit in the long wavelength range (hereafter “longwave radiation”) onto other urban surfaces or the sky. Longwave radiation is dependent on surface temperature, emissivity and view factors. The view factors are purely mathematical constructs that characterize how much a given surface can see the other surfaces. In particular the Sky View Factor (SVF) of a surface is the portion of the sky seen by the surface.

We wish to assess the accuracy of the TEB and SPUC formulae for shortwave and longwave radiation. The radiation values estimated by those two schemes will be compared to the hourly shortwave radiation (diffuse + direct) and longwave view factors determined for the *actual* geometry. As a reminder, the TEB model assumes infinitely long rows of identical buildings separated by infinitely long identical urban canyons. Therefore, the domain of study can be reduced to a 2D cross-section. Furthermore, using symmetry properties, it is possible to reduce the model to a single road and two opposing walls. The SPUC scheme, on the other hand, is 3-dimensional. It considers regularly positioned cuboid buildings. The cuboid buildings are identical and positioned in a regular grid-like array (i.e., same street width). It should be noted that in their description of the SPUC idealized geometry [Aoyagi and Seino \(2011\)](#), the authors only set forth formulae for view factors as well as shortwave beam radiation and its first specular reflection (i.e., diffuse radiation not considered). We have improved the scheme to include diffuse radiation as well as diffuse reflection of beam radiation beyond the first bounce. Said improvements were inspired by the TEB formulae.

The calculation of *actual* view factors and hourly global irradiance on all surfaces was conducted using the DIVA add-on on Grasshopper™ for Rhinoceros® ([Bachman, 2017](#)). For the calculation of the actual shortwave radiation a ray tracing simulation was executed on DIVA/Grasshopper for the *actual* urban case. A 5m x 5m grid was found to provide optimal accuracy. [Fig. 5](#) shows the total

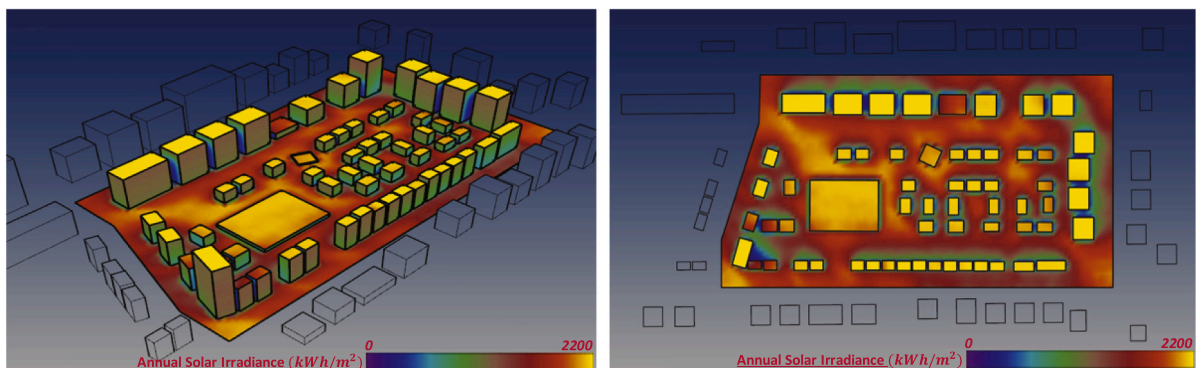


Fig. 5. Total incident short-wavelength irradiance on all surfaces for the actual urban case (total annual).

incident short-wavelength irradiance (hereafter referred to as “global irradiance”) on each urban surface.

Fig. 6 displays the annual global irradiance on roofs/façades/pavements for the rural and urban cases. The area-weighted average results per surface type are shown: hourly values for the whole year and average daily profiles for summer and winter. The urban TEB and SPUC irradiance values are presented in Fig. 7. It should be noted that the rural global irradiance on vertical façades is based on a cylindrical assumption for a stand-alone building (no shading from neighboring buildings). Its direct component is derived from the DNI (Direct Normal Irradiance) and the zenith angle while its diffuse component is a function of DHI (Diffuse Horizontal Irradiance) and GHI (Global Horizontal Irradiance) as described in standard solar radiation textbooks. The rural global irradiance on horizontal surfaces (roof, paved surfaces) is assumed to be identical with the GHI.

The irradiance values calculated by the SPUC formulas are quite different from the values derived from the standard TEB formulation. This is because TEB assumes that the urban domain consists of infinitely long rows of buildings (2D geometry) while SPUC assumes a 3D geometry of regularly positioned cuboids, as shown on Fig. 2. Furthermore, the standard TEB approach, used here, prescribes the integration of the street orientation from 0° to 360° so the calculated values are valid for a city in which streets have quasi-random orientation without any recognizable predominant orientation. SPUC formulas, on the other hand, assume a fixed rectangular grid of buildings/streets and are not easily amenable to the integration maneuver because of their complexity—so the selected orientation of the streets matters. In our case, we choose to rotate the streets by 45° from the cardinal directions because this is closest to the actual configuration of the streets in Abu Dhabi.

For paved surfaces, the SPUC solar scheme results in markedly higher mean global irradiance values, especially in winter with day-time average peaks of about 500 W/m² instead of 300 W/m² for TEB. When it comes to the mean global irradiance on the walls, SPUC predicts lower values in the summer, whereas TEB does not predict a significant difference between summer and winter. Furthermore, we can observe a more distinct double-peak profile for the mean wall irradiance calculated by SPUC for the wall in winter. When it comes to the pavement, in comparison to the TEB scheme, the modified SPUC solar radiation is higher, especially in winter. And the results for the roof are of course the same for both schemes because of the regularity of the buildings. In comparison to the actual data, the TEB results seem to be globally more accurate—although SPUC is slightly better for the pavement.

The view factors among urban surfaces and between urban surfaces and the sky are displayed in Table 3 for different models. The actual view factors are area-weighted averages per surface type. The last column corresponds to the empirical model of Leung and Steemers (2008).

When it comes to sky view factor SPUC shows better accuracy than TEB for the ground-to-sky value in comparison to the actual value estimated by DIVA/Grasshopper and Ecotect. For the walls, on the other hand, TEB is slightly more accurate. Leung and Steemers (2008) is most accurate for the ground but not for walls. The other sky view factors are derived using the usual relationships.

4.2. CFD-based adjustment of morphological and aerodynamic parameters

Using CFD to parametrize UCM is not new. As we saw previously, it has been done in the past to parametrize the MLUCM. However, in those cases the CFD simulation was transient and conducted for idealized geometries. Here, we suggest a site-specific flow-only steady-state RANS simulation. Specifically, we rely on the results of the simulation described in Ramirez et al. (2018). The simulation domain of that study consisted of a large portion of downtown Abu Dhabi comprising close to 1,400 buildings with a total ground area of approximately 3.6 km². The domain is long enough to capture how the low-level flow penetrates the city and wide enough to consider the influence of surrounding buildings. Rural hourly wind data from 2012 to 2015 were analyzed. Wind speed does not exhibit noteworthy seasonality in Abu Dhabi. The predominant wind direction at the rural station is north-north-west, with an average

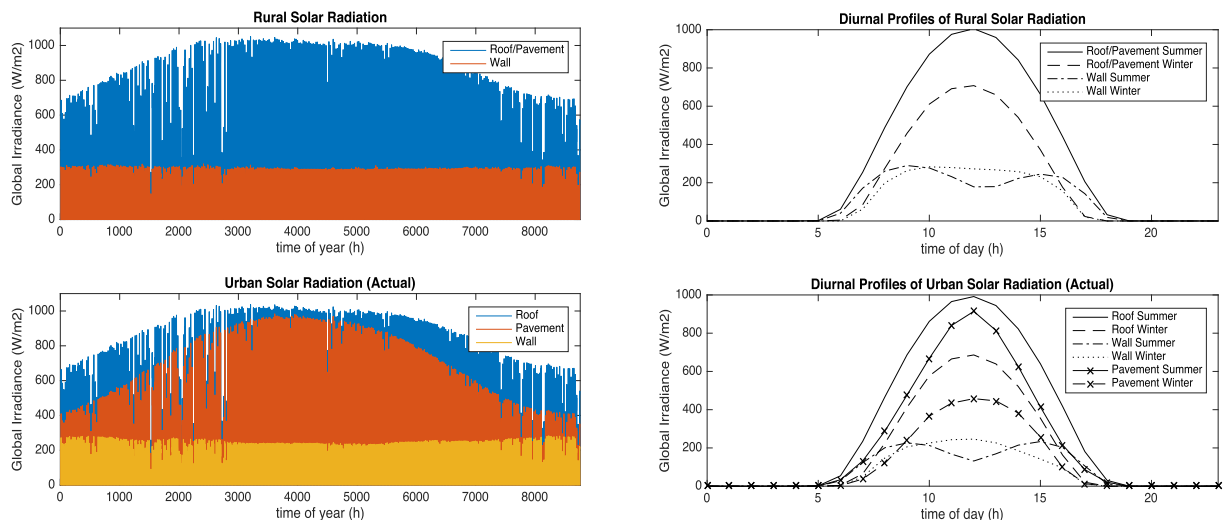


Fig. 6. Annual and diurnal global irradiance per surface type for the rural and actual urban cases.

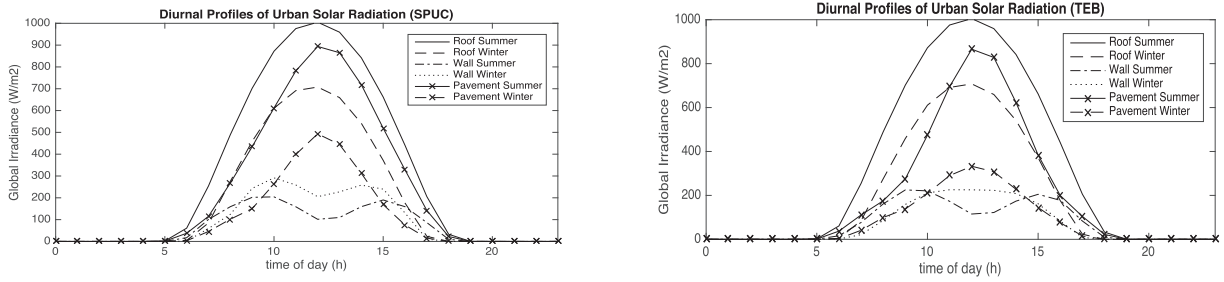


Fig. 7. Global irradiance per surface type for the SPUC (left) and TEB (right) schemes.

wind speed of 2.9 m/s at a height of 10 m above ground. Considering the atmospheric boundary layer and the scale at hand, these conditions were assumed to be similar in the immediate proximity of the city of Abu Dhabi, and were therefore used to derive the inlet boundary conditions of the computational domain. The inviscid wall condition was imposed to the lateral surfaces to make the computation more stable, i.e., the normal velocity component and normal gradients of tangential velocity components was set to zero. The boundary condition corresponding to the ground surface and building surfaces is non-slip, while the top of the domain is assumed to be a symmetry plane or pressure outlet due to the assumed parallel and horizontal behavior of the flow at those heights. At the outlet of the domain, zero static gauge pressure was imposed. The reader is referred to Ramirez et al. (2018) for additional details about the CFD simulation.

For our application, the “C Stripe” (which includes district E3), is of the most immediate interest. Based on the CFD simulation results, we suggest the following replacements for the default UCM parameters:

- $C_{dh} = 4.69$
- $d = 31.7$ m and $z_0 = 5.35$ m
- $z_b = 52.3$ m (this variable is referred to as z_1 in Ramirez et al. (2018))
- $z_{ref} = 90.3$ m (this variable is referred to as z_2 in Ramirez et al. (2018))
- $a = 1.60$
- $u_{ref}/u_a = 1.11$ as inferred from figure 5 of Ramirez et al. (2018)
- $u^*/u_{ref} = 0.143$
- $u_{top}/u_{ref} = 0.403$
- $u_{can}/u_{ref} = 0.171$

4.3. Urban canyon horizontal wind speed

As mentioned previously, our preferred source of weather data is IWEC. There is one exception to this rule and that is when it comes to the generation of the regression equation linking urban canyon wind speed to rural wind speed and other rural weather variables. Although this regression will be done for a period that is different from that of the IWEC data, our assumption is that given the rather immutable layout of Abu Dhabi’s inner downtown for at least the past 30 years, the inferred relationship has universal validity and can thereafter be applied to the IWEC rural data to reconstruct the urban wind velocity. The data used to fit the regression model correspond to the full year 2010 (8760 hourly values). The rural data was collected by a weather station located near the international airport. The urban data was collected by a roadside urban air monitored installed and operated by the Environmental Agency (24.488928°N, 54.363717°E). It is located immediately to the left of the E3 district as can be seen on Fig. 1. All data are of high quality.

For the estimation of the urban canyon wind speed from the rural wind speed, we use the stepwisefit function of Matlab, testing the significance of several rural weather station variables in the regression model. However, the algorithm retains as significant only the following rural variables: wind speed u_a , x and y components of u_a and ambient temperature T_a (in K). Thus, the regression equation gives the estimated value \hat{u}_{can} at time t as a function of several rural variables at the same time step:

$$\hat{u}_{can}(t) = b_0 + b_1u_a(t) + b_2u_{ax}(t) + b_3u_{ay}(t) + b_4T_a(t)$$

Table 3

View Factors.

	Actual	TEB	SPUC	Leung & Steemers
Ground to sky F_{ps}	0.60	0.38	0.67	0.63
Facade to sky F_{fs}	0.30	0.27	0.22	0.37
Roof to sky F_{rs}	0.94	1	1	1
Ground to facade F_{pf} (derived: $F_{pf} = 1 - F_{ps}$)	0.40	0.62	0.33	0.38
Facade to ground F_{fp} (derived: $F_{fp} = F_{fs}$)	0.30	0.27	0.22	0.37
Facade to facade F_{ff} (derived: $F_{ff} = 1 - 2F_{fs}$)	0.40	0.44	0.56	0.26

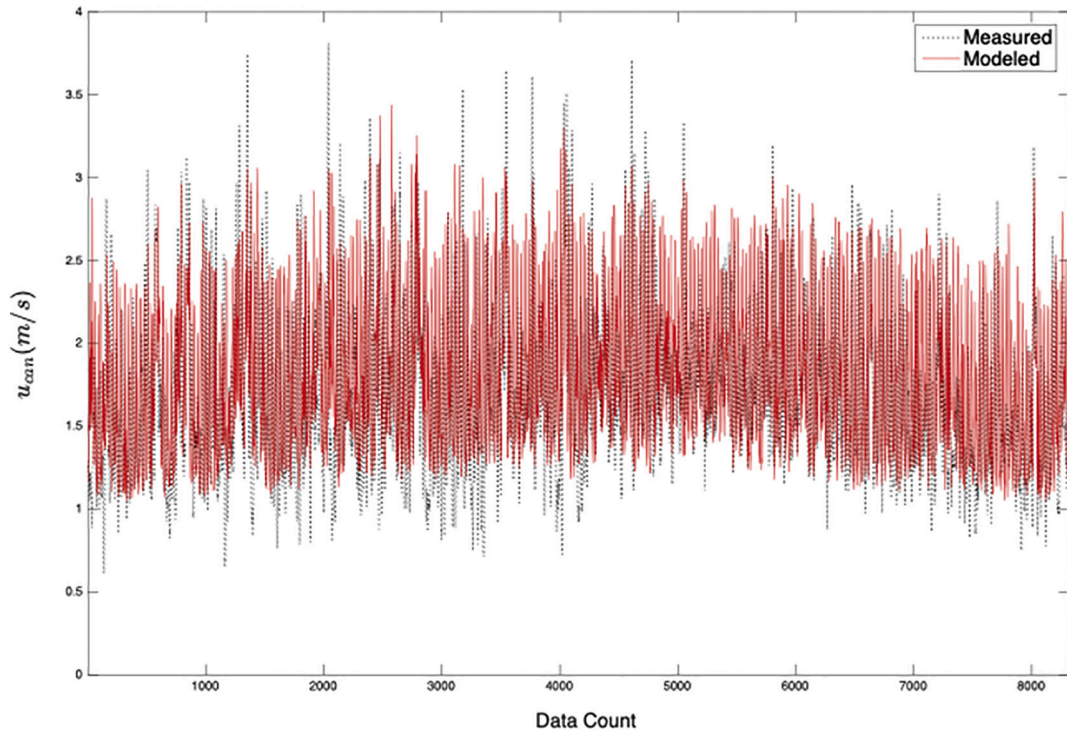


Fig. 8. Actual versus regressed urban wind speed (2010 data).

Before calculating the regression coefficients, we use a backward-looking moving average filter with a span of $8h$ to smooth the wind data. The first 8 data points are thereafter eliminated from the processed dataset. A certain level of smoothing is beneficial given the existence of data points corresponding to wind gust that are unlikely to be relevant to our urban canopy model. These infrequently occurring data points are very difficult to estimate accurately and, if left unprocessed, can significantly impact the least squares algorithm used in the estimation given their large values. When estimating the urban canyon wind speed from the EPW rural data, we will also filter, in the same way, the rural wind time series before feeding it to the regression model.

In addition, the results are much improved if the regression coefficients are separately estimated for different 3-h periods of the day. Specifically, we estimate a regression coefficient vector for the following periods: $[0h, 3h]$, $[3h, 6h]$, $[6h, 12h]$, $[12h, 15h]$, $[15h, 18h]$, $[18h, 21h]$ and $[21h, 24h]$. In other words, 8 sets of coefficients:

$$\begin{aligned}
 1st\ period : \quad & b = [-1.6020 \ 0.1296 \ 0.0630 \ 0.0275 \ 0.0098] \\
 2nd\ period : \quad & b = [-1.5568 \ 0.1525 \ 0.0631 \ 0.0862 \ 0.0094] \\
 3rd\ period : \quad & b = [-0.4380 \ 0.1907 \ 0.0458 \ 0.0483 \ 0.0052] \\
 4th\ period : \quad & b = [-0.1936 \ 0.1907 \ 0.0394 \ 0.0207 \ 0.0043] \\
 5th\ period : \quad & b = [-0.5498 \ 0.1296 \ 0.0390 \ -0.0149 \ 0.0059] \\
 6th\ period : \quad & b = [-0.3904 \ 0.0902 \ 0.0591 \ -0.0087 \ 0.0058] \\
 7th\ period : \quad & b = [1.0232 \ 0.1550 \ 0.0785 \ -0.0142 \ 0.0017] \\
 8th\ period : \quad & b = [-1.1835 \ 0.1250 \ 0.0565 \ -0.0282 \ 0.0083]
 \end{aligned}$$

The t-statistics of all of the coefficients are significant at the 95% confidence level. The overall Root Mean Square Error (RMSE) of the regression is 0.392 m/s. This is acceptable given that measured urban canyon wind speed already features a very high standard deviation of 0.657 m/s. Fig. 8 displays the actual and regressed values of the urban canyon wind velocity.

A scatter plot of modeled versus measured data is presented on Fig. 9. Although the overall bias of the model is nearly zero (0.067), the figure shows slight bias of the regression model in estimating lower and higher wind speeds.

5. Results

5.1. Baseline case

In the baseline case, to which the “improved” cases will be compared henceforth, we use the presumably more accurate *actual* radiation and *CFD-derived* morphological/aerodynamic parameters in the UCM. In that sense, the baseline case represents the fully

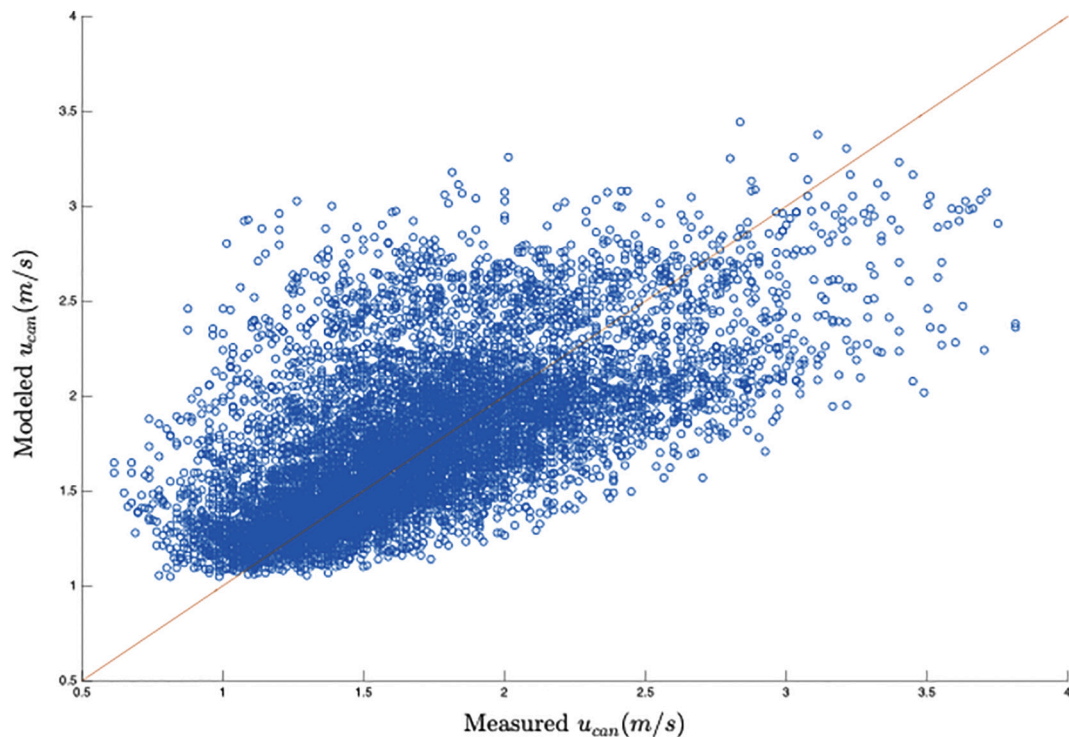


Fig. 9. Scatter plots of regressed versus measured urban wind speed.

improved model—with the exception of canyon wind speed improved, which is treated slightly differently—and we evaluate the impact of each of the first two improvements, by discarding it from the fully improved model and using a corresponding “standard” approach instead. The standard approach for radiation is to use the TEB or the SPUC scheme. For morphological parameters, it consists in using standard morphometric formulae described in Section 3.2.

For the baseline case, we obtain, after an annual hourly simulation (8760 h) driven by the EPW rural measurements, average cooling electricity consumption per floor area of 152 kWh/m^2 with a peak cooling electricity demand of 51.8 W/m^2 . The annual average of the hourly UHI intensity for the same EPW data is 1.69 K . This is consistent with average values measured in recent years by the authors in different locations in Abu Dhabi, as compared to a university-operated rural weather station near the international airport. The modeled annual average diurnal profile of UHI intensity for the baseline case is shown on Fig. 10. On the same figure, the actual average profile of UHI intensity measured over a recent 18-month period by one of the downtown monitoring stations is shown (together with its standard deviation). The actual UHI intensity is determined as the differential between the urban temperature and the aforementioned university-operated rural station. The average diurnal profiles of the different atmosphere-canopy energy fluxes, calculated by the baseline model, are shown on Fig. 11 where positive values signify energy received by the urban canopy.

5.2. Radiation improvement

If we use the TEB radiation parameters in the UCM, we obtain average cooling electricity consumption per floor area of 149 kWh/m^2 with a peak cooling electricity demand of 49.7 W/m^2 . The average annual UHI intensity is 1.61 K . If we use the SPUC radiation parameters in the UCM, we obtain average cooling electricity consumption per floor area of 161 kWh/m^2 with a peak cooling electricity demand of 52.2 W/m^2 . The average annual UHI intensity is 1.81 K . Generally, using the TEB radiation parameters results in an underestimation while the TEB radiation parameters cause an overestimation. However, SPUC is more accurate than TEB when it comes to UHI intensity and peak cooling demand. The canyon wind velocity is unchanged. The results are displayed in Table 4. Generally, the SPUC radiation scheme is worse than TEB, except for the peak cooling demand. TEB underestimates while SPUC overestimates.

5.3. CFD-driven improvement

If we replace the CFD-driven parameters (extracted from Ramirez et al., 2018, “Stripe C”) with their default empirically calculated values, we obtain average cooling electricity consumption per floor area of 156 kWh/m^2 with a peak cooling electricity demand of 52.6

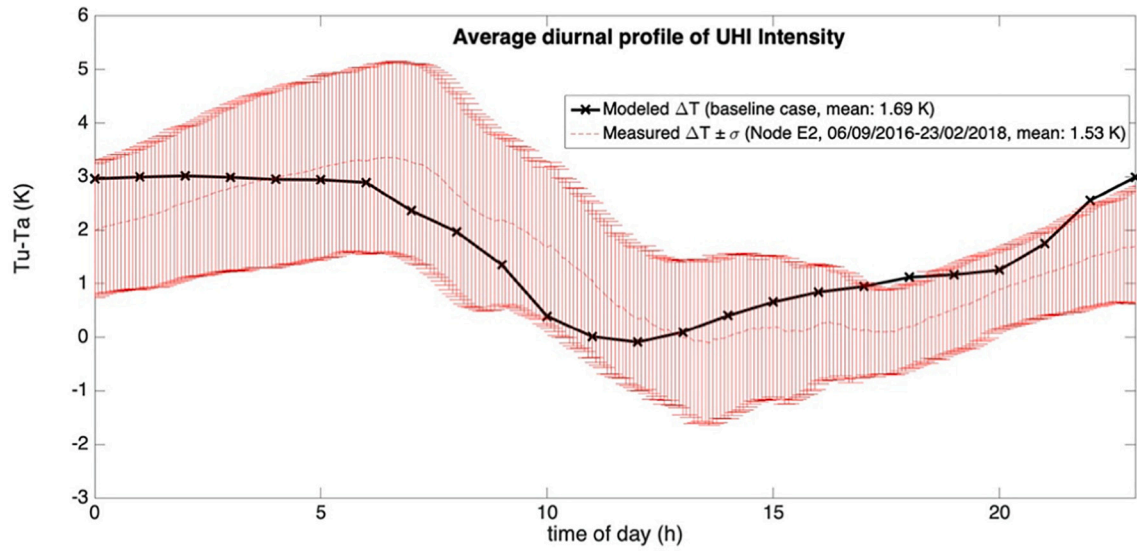


Fig. 10. Average Diurnal profile of the UHI intensity in the baseline scenario.

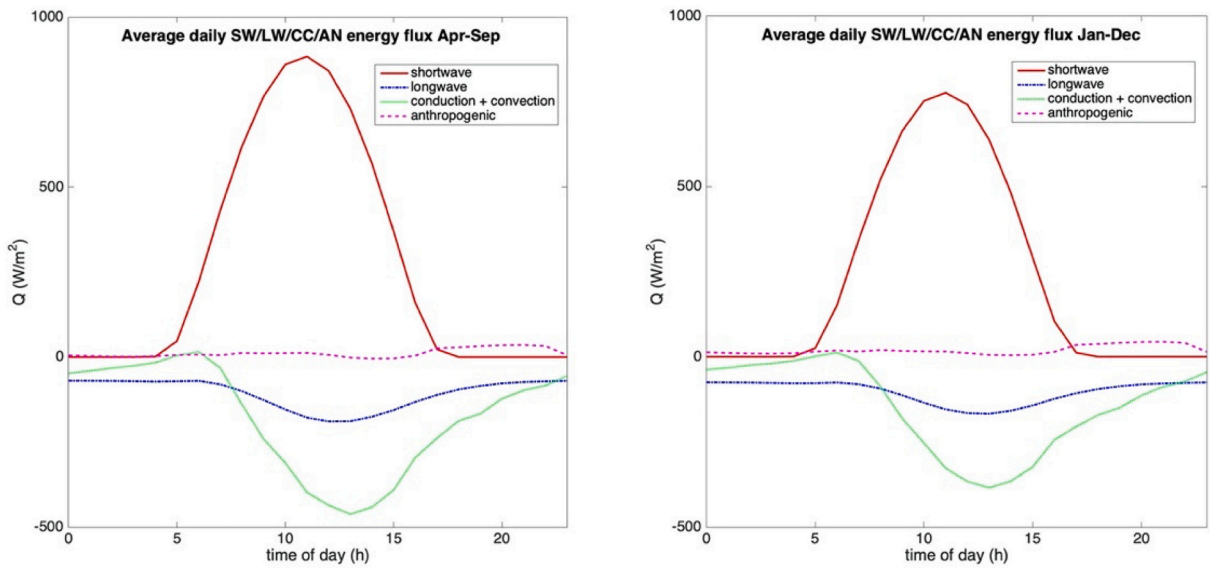


Fig. 11. Average Diurnal profile of atmosphere-canopy energy fluxes in the baseline scenario, for summer months Apr.-Sep. (left) and for winter months Jan.-Dec. (right).

Table 4
Radiation impact.

	Baseline	TEB	SPUC
Cooling electricity use (kWh/m ²)	152	149	161
Cooling peak demand (W/m ²)	51.8	49.7	52.2
Average annual UHI intensity (K)	1.69	1.61	1.81
		-2.0%	+7.1%
		-4.1%	+0.8%
		-4.7%	+7.1%

Table 5
CFD impact.

	Baseline	Non-CFD
Cooling electricity use (kWh/m ²)	152	156 +2.6%
Cooling peak demand (W/m ²)	51.8	52.6 +1.5%
Average annual UHI intensity (K)	1.69	2.06 +22%
Average canyon wind speed (m/s)	1.64	1.68 +2.4%

W/m². The average annual UHI intensity drastically increases to 2.05 K. The canyon wind velocity is overestimated by 2.4%. Generally, using empirical formulae instead of presumably more accurate RANS-derived parameters results in an overestimation. In particular the average annual UHI intensity is significantly impacted, with an overestimation exceeding 20%. The impact on the other indicators is much smaller. The results are displayed in Table 5.

5.4. Wind velocity improvement

If we replace, in the baseline case, the Masson (2000) approximation of the canyon wind speed with the one regressed from rural wind speed, we obtain average cooling electricity consumption per floor area of 153 kWh/m² with a peak cooling electricity demand of 51.7 W/m². The average annual UHI intensity is 1.68 K. The canyon wind velocity is 1.87 m/s. The impact on all indicators except wind speed is very small. The results are displayed in Table 6.

6. Discussion and conclusion

The main contribution of this study is the assessment of the impact of several original improvements to an existing urban canopy model by replacing default schemes and parameters with more accurate ones determined in consideration of prior information about the actual urban district under consideration. The comparisons are conducted for a real district in downtown Abu Dhabi for which GIS data is available and a prior steady-state CFD simulation was conducted. Furthermore, historical urban wind speed measurements are available for the district. Specifically, we evaluate the benefits of using three improvements in the UCM: 1) Replacing radiation parameters derived from the TEB (Town Energy Balance) or the SPUC (Square Prism Urban Canopy) schemes by the *actual* values calculated in Grasshopper for the real geometry; 2) Replacing morphological/aerodynamic parameters estimated by usual empirical formulae by CFD-derived values; 3) Replacing the canyon wind speed estimated by the logarithmic + exponential formula of Masson (2000) by the value inferred from the rural measurements, according to a regression model fitted to historical data.

Initially, we validate TEB and SPUC radiation schemes by comparing to *actual* values. It is notable that the SPUC scheme has been improved in our study to include diffuse radiation as well as diffuse reflection of beam radiation beyond the first bounce. As far as Sky View Factor (SVF) estimates are concerned, SPUC is more accurate than TEB. SPUC is more accurate for the ground SVF while TEB is better for the façade SVF. For the roof SVF, it is acceptable to use 1 in most usual cases. The empirical model of Leung & Steemers is slightly superior to both TEB and SPUC. Further, we looked at shortwave radiation and its impact on urban canopy model accuracy. The modified SPUC solar radiation is generally higher for the ground in winter and lower for the walls in summer. While it can be presumed that, here too, SPUC should perform better than TEB given that the cuboid geometry is closer to the real geometry than TEB's infinite urban canyons, the performance (i.e., the accuracy of the UHI and cooling energy/demand indicators) of TEB is better than that of SPUC with the exception of the peak cooling demand. Overall, replacing TEB/SPUC estimations by *actual* radiation values do not have a significant impact on the results of the UCM simulation.

The second improvement tested in this study consisted in replacing standard formulae expressing morphological parameters as a function of the primary parameters h , λ_p and λ_f with correlations derived from a prior steady-state RANS simulation. More precisely, we evaluated the performance penalty of *not* using CFD-derived values in the UCM. The impact of this improvement is more significant than the radiation improvement. By using the standard relations instead of RANS-derived values, we overestimate the UHI intensity by a staggering 22%. Of course, one can try to reduce this performance penalty by switching the empirical relations with others reported in the literature that work better. However, although this approach may indeed result in a reduction of the penalty in this particular site, there is no guarantee that if the UCM is applied to a different site, the gain will persist. The cooling energy indicators are not significantly impacted by this improvement. Also, the empirical relations seem to predict urban canyon wind speed rather accurately, when compared to CFD.

The final improvement concerns the urban canyon wind speed estimation. In this case, the higher accuracy of the regressed estimate is debatable. Therefore, in this case, we simply report the performance changes and do not comment on accuracy. The regressed wind speed itself is higher by about 12% when compared to the baseline case. The other performance indicators are almost unchanged

Table 6
Canyon wind speed impact.

	Baseline	Regressed u_{can}
Cooling electricity use (kWh/m ²)	152	153 +0.7%
Cooling peak demand (W/m ²)	51.8	51.7 -0.2%
Average annual UHI intensity (K)	1.69	1.68 -0.6%
Average canyon wind speed (m/s)	1.64	1.87 +14%

(less than 1% change). Remarkably, the cooling energy is exactly the same as in the baseline case.

In conclusion, in the absence of GIS data enabling the calculation of actual radiation values, selecting the TEB scheme does not result in significant errors, although the UHI intensity may be off by about 5%. In the more likely case of lacking CFD simulation results, the UHI can be significantly off—by more than 20%. It is possible that choosing alternate empirical morphometric relations may decrease that error, however this improvement is unlikely to be universal. Regressed urban canyon speed is, as could be expected, quite different from the default canyon speed estimation. But the impact on UHI/cooling performance indicators is negligible.

Declaration of Competing Interest

The authors declare that they have no known competing financial interests or personal relationships that could have appeared to influence the work reported in this paper.

Acknowledgement

This research was mainly supported by the Fraunhofer Internal Programs under Grant No. Attract 003-695033 (Germany). The development of the software was funded, in part, by a previous grant under the Cooperative Agreement between the Masdar Institute of Science and Technology and the Massachusetts Institute of Technology, Grant No. 02/MI/MIT/CP/11/07633/GEN/G/00 (United Arab Emirates).

Appendix A. Mascart formulations

Using empirical formulations, we can express C_D and C_H in terms of their respective ‘neutral conditions’ (no buoyancy) values:

$$C_D = C_{DN} F_M$$

$$C_H = C_{HN} F_H$$

The neutral limit values C_{DN} and C_{HN} are easily derived from the standard expressions of C_D and C_H by setting $\Psi_M = \Psi_H = 0$:

$$C_{DN} = \left(\frac{\kappa}{\ln\left(\frac{z-z_d}{z_0}\right)} \right)^2$$

$$C_{HN} = \frac{1}{R} \left(\frac{\kappa}{\ln\left(\frac{z-z_d}{z_0}\right)} \right)^2 = \frac{C_{DN}}{R}$$

As for F_M and F_H , according to Mascart et al. (1995), they can be expressed as functions of the bulk Richardson number $Ri = \frac{g z \Delta \theta}{\theta u^2}$:

$$\left\{ \begin{array}{l} \text{Unstable conditions } (Ri \leq 0) : \quad F_M = 1 - \frac{b Ri}{1 + C_m \sqrt{|Ri|}}; \quad F_H = \eta \left(1 - \frac{b Ri}{1 + C_h \sqrt{|Ri|}} \right) \\ \text{Stable conditions } (Ri > 0) : \quad F_M = \frac{1}{(1 + b' Ri)^2}; \quad F_H = \frac{\eta}{(1 + b' Ri)^2} \end{array} \right.$$

where:

$$b = 2b' = 9.4$$

$$\eta = \left[\ln \left(\frac{z-d}{z_0} \right) / \ln \left(\frac{z-d}{z_{0H}} \right) \right], \mu = \ln \left(\frac{z_0}{z_{0H}} \right)$$

$$C_m = C_m^* C_{DN} b \eta \left(\frac{z-d}{z_0} \right)^{p_m}, C_h = C_h^* C_{DN} b \eta \left(\frac{z-d}{z_{0H}} \right)^{p_h}$$

$$C_m^* = 6.874 + 2.6933 \mu - 0.3601 \mu^2 + 0.0154 \mu^3$$

$$C_h^* = 3.2165 + 4.3431 \mu + 0.536 \mu^2 - 0.0781 \mu^3$$

$$p_m = 0.5233 - 0.0815 \mu + 0.0135 \mu^2 - 0.001 \mu^3$$

$$p_h = 0.5802 - 0.1571 \mu + 0.03271 \mu^2 - 0.0026 \mu^3$$

References

- Abu Dhabi Municipality, 2011. Energy Consumption Management Program in Existing Buildings, unpublished report, 31 October 2011.
- Afshari, A., 2017. A new model of urban cooling demand and heat island—application to vertical greenery systems (VGS). *Urban Clim.* 157, 204–217.
- Afshari, A., Nikolopoulou, C., Martin, M., 2014. Life-cycle analysis of building retrofits at the urban scale—a case study in United Arab Emirates. *Sustainability* 6, 453–473.
- Afshari, A., Schuch, F., Marpu, P., 2018. Estimation of the traffic related anthropogenic heat release using BTEX measurements – a case study in Abu Dhabi. *Urban Clim.* 24, 311–325.
- Aoyagi, T., Seino, N., 2011. A square prism urban canopy scheme for the NHM and its evaluation on summer conditions in the Tokyo metropolitan area, Japan. *J. Appl. Meteorol. Climatol.* 1476–1496.
- Bachman, D., 2017. Grasshopper: Visual Scripting for Rhinoceros 3D. Industrial Press.
- Beljaars, A.C.M., Holtlag, A.A.M., 1991. Flux parameterization over land surfaces for atmospheric models. *J. Appl. Meteorol.* 30, 327–341.
- Bottema, M., 1997. Urban roughness modelling in relation to pollutant dispersion. *Atmos. Environ.* 31 (18), 3059–3075.
- Bueno, B., Norford, L., Hidalgo, J., Pigeon, G., 2013. The urban weather generator. *J. Build. Perform. Simul.* 269–281.
- Businger, J.A., Wyngaard, J.C., Izumi, Y., Bradley, E.F., 1971. Flux-profile relationships in the atmospheric surface layer. *J. Am. Meteorol. Soc.* 28, 181–189.
- Chen, F., Kusaka, H., Bornstein, R., Ching, J., et al., 2011. The integrated WRF/urban modeling system: development, evaluation, and applications to urban environmental problems. *Int. J. Climatol.* 31, 273–288.
- Cionco, R.M., 1965. A mathematical model for air-flow in a vegetative canopy. *J. Appl. Meteorol.* 4, 517–522.
- Erell, E., Pearlmutter, D., Williamson, T., 2010. *Urban Microclimate: Designing the Spaces between Buildings*. Routledge.
- Gabriel, K.M.A., Endlicher, W.R., 2011. Urban and rural mortality rates during heat waves in Berlin and Brandenburg, Germany. *Environ. Pollut.* 159, 2044–2050.
- Garratt, J.R., 1992. *The Atmospheric Boundary Layer*. Cambridge University Press.
- Grimmond, C.S.B., Oke, T.R., 1999. Aerodynamic properties of urban areas derived from analysis of surface form. *J. Appl. Meteorol.* 38, 1262–1292.
- Grossman-Clarke, S., Zehnder, J.A., Stefnov, W.L., Liu, Y., Zoldak, M.A., 2005. Urban modifications in a Mesoscale meteorological model and the effects on near-surface variables in an arid metropolitan region. *J. Appl. Meteorol.* 1281–1297.
- Hogstrom, U., 19. Non-dimensional wind and temperature profiles in the atmospheric surface layer - A re-evaluation. *Bound. Layer Meteorol.* 42, 55–78.
- Jacobson, M.Z., 2005. *Fundamentals of Atmospheric Modeling*, Second edition. Cambridge University Press.
- Jänicke, B., Meier, F., Fenner, D., Fehrenbach, U., Holtmann, A., Scherer, D., 2017. Urban–rural differences in near-surface air temperature as resolved by the Central Europe refined analysis (CER): sensitivity to planetary boundary layer schemes and urban canopy models. *Int. J. Climatol.* 37, 2063–2079.
- Jürges, W., 1924. The heat transfer at a flat wall (Der Wärmeübergang an einer ebenen Wand). *Beihefte zum Gesundh.-Ing.* 1 (19).
- Huang, J., Jones, P., Zhang, A., Peng, R., Li, X., Chan, P., 2020. Urban Building Energy and Climate (UrBEC) simulation: Example application and field evaluation in Sai Ying Pun, Hong Kong. *Energy Build.* 207, 2044–2050.
- Kusaka, H., Kondo, H., Kikigawa, Y., Kimura, F., 2001. A simple single-layer urban canopy model for atmospheric models: comparison with multi-layer and slab models. *Bound. Layer Meteorol.* 329–358.
- Landsberg, H.E., 1981. *The Urban Climate*. Academic Press.
- Le Bras, J., Masson, V., 2015. A fast and spatialized urban weather generator for long-term urban studies at the city-scale. *Front. Earth Sci.* 3, 27.
- Leung, K., Steemers, K., 2008. Estimating Average Sky View Factors of Urban Surfaces with Simple Geometric Parameters. PLEA, Dublin.
- Liu, Y., Chen, F., Warner, T., Basara, J., 2006. Verification of a mesoscale data-assimilation and forecasting system for the Oklahoma City area during the Joint Urban 2003 field project. *J. Appl. Meteorol.* 912–929.
- Louis, J.E., 1979. A parametric model of vertical Eddy fluxes in the atmosphere. *Bound.-Layer Meteorol.* 17, 187–202.
- Maronga, B., Banzhaf, S., Burmeister, C., Esch, et al., 2020. Overview of the PALM model system 6.0. *Geosci. Model Dev.* 13, 1335–1372.
- Martilli, A., Clappier, A., Rostach, M.W., 2002. An urban surface exchange parameterization for mesoscale models. *Bound. Layer Meteorol.* 261–304.
- Mascart, P., Noilhan, J., Giordani, H., 1995. A modified parameterization of flux-profile relationships. *Bound.-Layer Meteorol.* 72, 331–344.
- Masson, V., 2000. A physically-based scheme for the urban energy budget in atmospheric models. *Bound.-Layer Meteorol.* 357–397.
- Melecio-Vázquez, D., Ramamurthy, P., Arend, M., et al., 2018. Thermal structure of a coastal–urban boundary layer. *Bound. Layer Meteorol.* 169, 151–161.
- Mirzaei, P., 2015. Recent challenges in modeling of urban heat island. *Sustain. Cities Soc.* 200–206.
- Monin, A., Obukhov, A., 1954. Basic laws of turbulent mixing in the atmosphere near the ground. *Tr. Akad. Nauk SSSR Geofiz. Inst.* 24, 163–187.
- Nazarian, N., Krayenhoff, E.S., Martilli, A., 2020. A one-dimensional model of turbulent flow through ‘urban’ canopies (MLUCM v2.0): updates based on large-eddy simulation. *Geosci. Model Dev.* 13 (3), 937–953.
- Oke, T.R., 1973. *City Size and Urban Heat Island*. Atmospheric Environment Pergamon Press, pp. 769–779.
- Panagiotou, I., Neophytou, M.K.-A., Hamlyn, D., Britter, R.E., 2013. City breathability as quantified by the exchange velocity and its spatial variation in real inhomogeneous urban geometries: an example from central London area. *Sci. Total Environ.* 442, 466–477.
- Pinterić, M., 2017. *Building Physics, from Physical Principles to International Standards*. Springer.

- Powers, J.G., et al., 2017. The weather research and forecasting model: overview, system efforts, and future directions. *Bull. Amer. Meteor. Soc.* 98, 1717–1737.
- Ramirez, N., Afshari, A., Norford, L., 2018. Validation of simplified urban-canopy aerodynamic Parametrizations using a numerical simulation of an actual downtown area. *Bound. Layer Meteorol.* 168, 155–187.
- Raupach, M.R., Thom, A.S., Edwards, I., 1980. A wind-tunnel study of turbulent flow close to regularly arrayed rough surfaces. *Bound.-Layer Meteorol.* 18, 373–397.
- Santiago, J.L., Martilli, A., 2010. A dynamic urban canopy parameterization for mesoscale models based on computational fluid dynamics Reynolds-averaged Navier–stokes microscale simulations. *Bound. Layer Meteorol.* 137, 417–439.
- Simón-Moral, A., Santiago, J.L., Krayenhoff, E.S., Martilli, A., 2014. Streamwise versus spanwise spacing of obstacle arrays: parametrization of the effects on drag and turbulence. *Bound.-Layer Meteorol.* 151, 579–596.
- Stull, R., 2017. *Practical Meteorology, an Algebra-Based Survey of Atmospheric Science*. UBC.
- Tsiringakis, A., Steeneveld, G.-J., Holtslag, A.A.M., Kotthaus, S., Grimmond, S., 2019. On- and off-line evaluation of the single-layer urban canopy model in London summertime conditions. *Q. J. R. Meteorol. Soc.* 145, 1474–1489.
- UWYO, 2020. University of Wyoming Atmospheric Soundings Web Site. University of Wyoming. <http://weather.uwyo.edu/upperair/sounding.html> (accessed 04.09.2020).